CHAPTER-4

Comparison of crystalline/crystalline interfaces in Au/Cu thin films on reversing the multilayer sequence

Chapter 4.
Comparison of crystalline/crystalline interfaces in Au/Cu thin films on reversing the multilayer sequence

4.1 Introduction

Interconnects are the key components to make contacts between the electronic devices [100,126,222,263–267]. Alloys or thin films of Au-Cu system are used for their manufacturing [64,223]. It is important to note that in which way the interconnects are made and applied. Such information helps in understanding the mechanism for microstructure evolution, and phase transformations [42,179]. This also facilitates the study of nature and behaviour of interfaces [98,227]. Delineating such criticalities requires extensive characterization and comparison of these alloys or thin films synthesized differently. Depending on the design of the electronic components and devices, the sequence of multilayer deposition may change [140,226,267]. Sometimes the Cu layer is sandwiched between the Au layers and vice-versa. However, the deposition of Au on Cu is always preferred as it protects Cu from oxidation. [227]. The overall performance of the electronic devices such as cell phones, ear plugs, printed circuit boards etc., depends on the efficacy of the interconnects. Therefore, the synthesis and design of such interconnects are considered to be the most crucial step for the smooth functioning of the electronic components and devices. This requires in-depth grasp of the equilibrium phase diagram of Au-Cu system as mentioned in chapter 3.

Absence of clear understanding about the changes in the Au-Cu phase diagram at nanometer length scale, the effect of non-equilibrium processing techniques on the phase and microstructural stability of Au-Cu multilayer is scarce [231]. Naturally, very limited information does exist in literature about the structure and chemistry of the interfaces in multilayers [44,49,148,235]. In order to address such issues, the Au/Cu multilayers have been explored and explained in chapter 3. The phase and microstructure evolution have been investigated by utilizing various techniques and it has been reported in chapter 3. In

this chapter, the consequence of changing the deposition sequence of Cu and Au is being explored for comparison vis-à-vis those reported in chapter 3.

4.1 Experimental Methods

In this chapter, the synthesis of 40TCu specimen is done. The details of the starting materials and their cleaning process are given in chapter 2 (section 2.2.1). The deposition sequence for sample designation (40TCu) is also mentioned in the table 2.1 of the same chapter. For the deposition of (40TCu) specimen through thermal evaporation technique, same procedure is followed as discussed in chapter 3 (section 3.2.1). Only the deposition sequence is reversed to the one taken in chapter 3.

4.2 Results

Figure 4.1 is the multiple display of experimentally obtained GIXRD patterns of 40TCu and 40TAu samples (top two patterns) along with the simulated patterns of Au, Cu and intermetallic phases. The experimental GIXRD pattern in figure 4.1 comes from a different sample in a different experiment. So its appearance is different from the GIXRD pattern reported in chapter 3 in figure 3.2. However, they present similar scientific information. On comparing the experimental patterns of both the samples with each other, a few less-prominent peaks are observed in the 40TCu pattern. The dotted lines are drawn in order to see how closely the peaks are matching for the experimental and the simulated patterns. The results show that the 40TCu pattern is predominantly matching with Cu simulated pattern and 40TAu pattern is predominantly matching with Au simulated pattern. Moreover, the simulated peaks of other intermetallic phases such as oP8 (AuCu), tP4 (AuCu), oI40 (AuCu), and cP4 (Au_3Cu or Cu_3Au) are also falling under the broadening of the experimental peaks of 40TCu and 40TAu. Additionally, the peaks in the 40TCu experimental pattern, which do not match either with Au or Cu simulated pattern, are found to be closer to the simulated peaks of intermetallic phases. Therefore, the existence of intermetallic phases cannot be ruled out in both the multilayered thin film specimens.

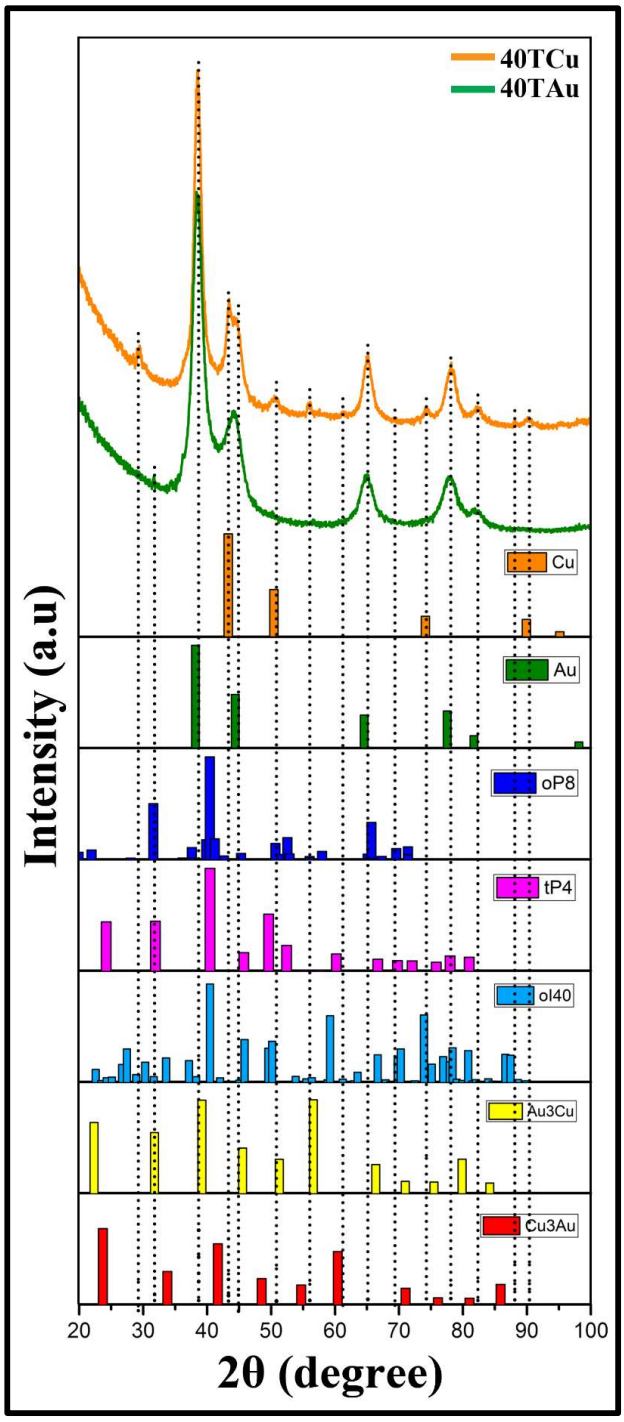

Figure 4.1: *Comparison of experimental GIXRD patterns (top two) of Au/Cu multilayer thin films with the simulated patterns of Au-rich (solid solution), Cu-rich (solid solution) and their intermetallics.*

The broadening of peaks in the experimental patterns of both specimens is attributed to the presence of small crystallites and non-uniform strain in the multilayered thin films. A little shift in the simulated peaks of the intermetallic phases from the exact Bragg peak positions (dotted lines) is attributed to the coexistence of multiple phases, stoichiometry and defects in the multilayered thin films. The unmatched simulated peaks of the intermetallic phases with the experimental peaks may be a result of their low volume fraction, high relative background noise, low form factor etc. The above GIXRD investigations reveals that the multilayered thin films in both the specimens mostly display solid solution of Au and Cu along with the presence of intermetallic phases in very low volume fraction. Such an observation is akin to those of chapter 3.

The bright field transmission electron microscope (BFTEM) images acquired from the cross-section specimens 40TCu and 40TAu are depicted in the figures 4.2a and 4.2b respectively for comparison. The multilayered film and the substrate regions are marked separately in both the specimens as shown in figures 4.2a and 4.2b. Moreover, within the film region for both of the specimens, individual layers with bright and dark crystallographic contrast can be seen. However, in the specimen 40TCu (Figure 4.2a), a layer just above the substrate is showing strong crystallographic contrast (black) whereas in the 40TAu specimen (Figure 4.2b) this layer is showing weak crystallographic contrast (white). It has also been observed in both of these specimens (Figure 4.2a and 4.2b) that the upper black layer is thicker than the lower black layer. The length ~ 100 nm at the surface of the thick black layer in figure 4.2a (marked with orange line) attains ~ 5 number of undulations whereas in figure 4.2b it is measured to be ~ 8 number of undulations.

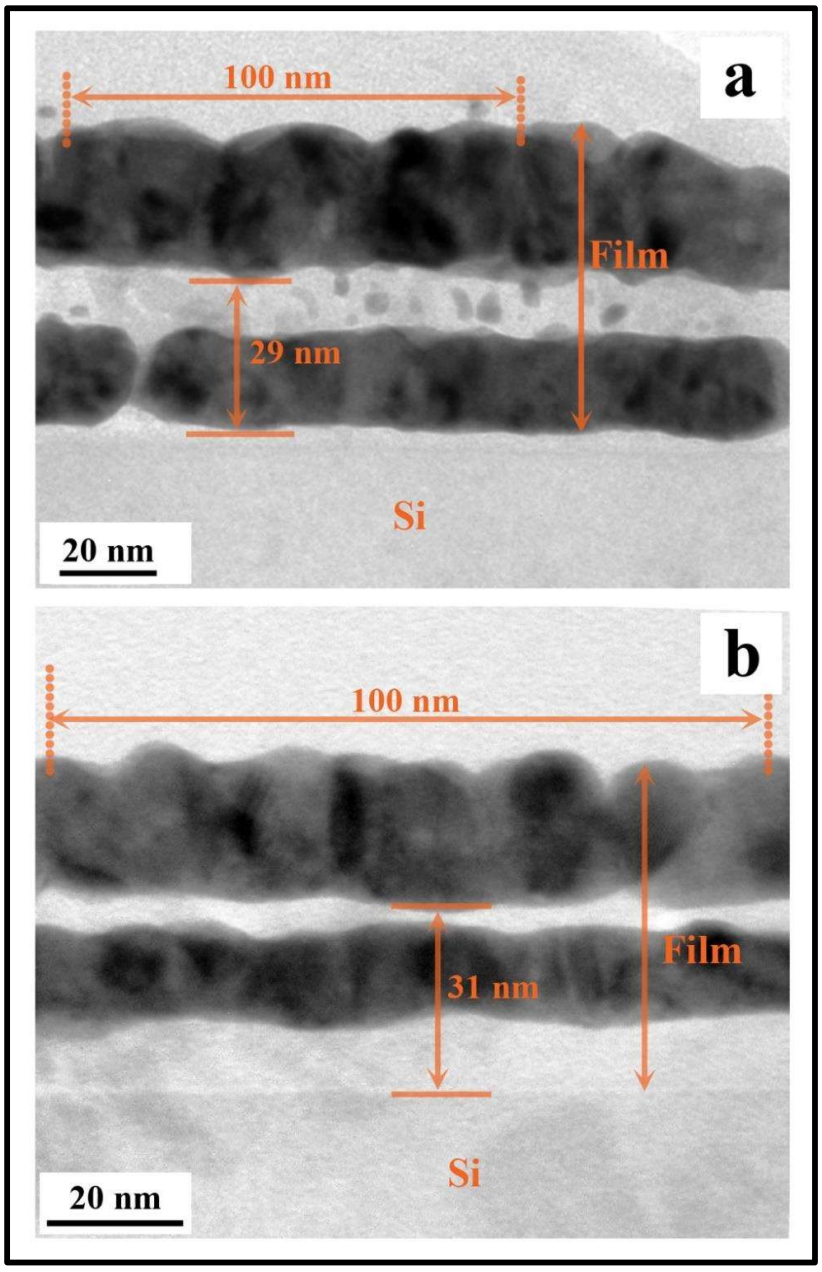

Figure 4.2: *Cross-section bright field (BFTEM) image of Au/Cu multilayer thin films* ***a)*** *40TCu specimen and,* ***b)*** *40TAu specimen.*

In addition to this, the distance of the interface from the substrate is also measured in both the specimens. This distance is measured to be ~ 29 nm in case of 40TCu specimen (Figure 4.2a) whereas it is ~31 nm in case of 40TAu specimen (Figure 4.2b). The overall

morphology of the multilayered thin films in case of both the specimens is observed to be columnar and governed by the black layers. The interruptions in the columnar morphology were found due to the presence of bright layers. The presence of bright layers in both the specimens is expected to be predominantly amorphous in nature by their appearance. In order to understand the chemistry of the multilayer thin films for 40TCu specimen, STEM-EDS experiments akin to those mentioned in chapter 3 has been done.

Figure 4.3a represents the HAADF image, STEM-EDS mapping and the line profile of the 40TCu specimen. In the HAADF image, film and substrate region is separately marked. The region selected for the STEM-EDS mapping in this specimen is shown with a red (unfilled) box marked in the HAADF image. The chemical spectrum generated from this region shows uniform distribution of Au and Cu elements in the multilayers. The dark (black) layer in the HAADF image of this specimen is rich in Cu and lean in Au. The two line profiles obtained from the multilayers have been shown alongside in the figure 4.3a. The vertical scan (yellow arrow pointing downwards) is done across the multilayer in order to determine the chemistry of the entire multilayer. The horizontal scan (yellow arrow pointing right) is done along the dark (black) contrast layer in order to determine its chemistry. The line profile corresponding to the vertical scan reveals that within the initial few nanometers distance (~ 20 nm) from the surface in the multilayer, the counts of Cu is more compared to the Au. However, as the line scan progressed, the counts of the Au became more than the Cu. This trend continues upto ~ 60 nm length and after this a gradual drop in the curves for both Au and Cu is observed.

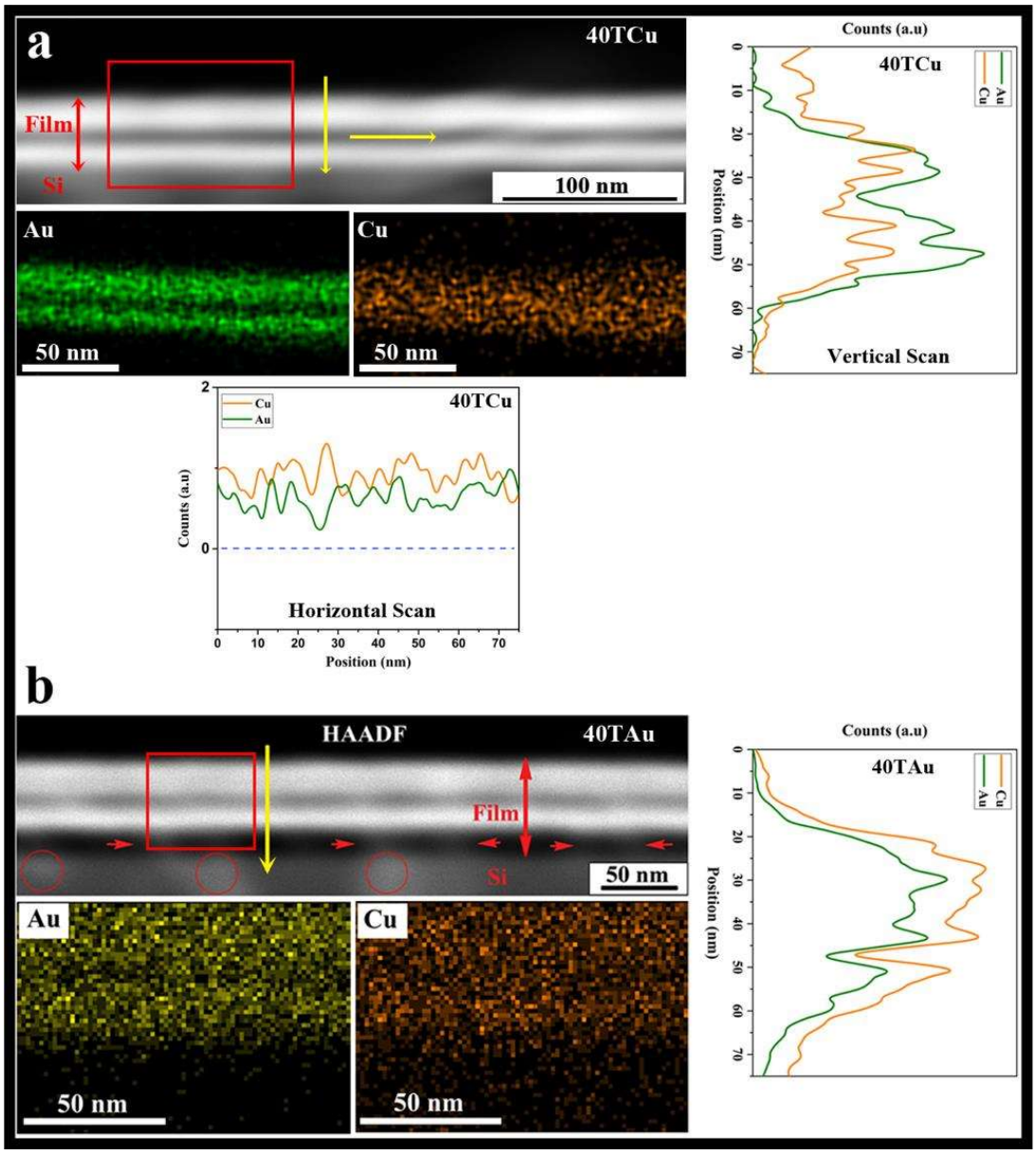

Figure 4.3: a) *Cross-section HAADF image of Au/Cu multilayer in 40TCu specimen along with the horizontal scan profile (showing Au and Cu counts), vertical scan profile (showing Au and Cu counts) and, STEM-EDS mapping (showing Au and Cu elemental distribution).* ***b)*** *Cross-section HAADF image of Au/Cu multilayer in 40TAu specimen along with the vertical scan profile (showing Au and Cu counts) and, STEM-EDS mapping (showing Au and Cu elemental distribution).*

The line scan corresponding to the horizontal scan reveals the presence of both the Au and Cu elements. The counts of the Cu element throughout the line scan length is more than the Au element. This indicates that the dark contrast (black) layer is Cu rich layer.

Figure 4.3b represents the HAADF image, STEM-EDS mapping and the line profile of the 40TAu specimen. This is given here to facilitate discussion for comparison with that of 40TCu. In the HAADF image, film and substrate region is separately marked. The region chosen for the chemical mapping is marked with the red color box (unfilled) within the multilayered film. The spectrum profile shows that the Au and Cu are uniformly distributed within the multilayered film. On carefully observing the spectrum, it has been observed that the dark (black) layers in the HAADF image are comparatively rich in Cu and few crystalline Cu clusters are observed (indicated by red arrows). In addition to this the Cu atoms seem to diffuse into the substrate (poly-Si), which can be seen in the same HAADF image (marked by unfilled red circles). The line profile of the multilayers is shown alongside in the figure 4.3b. Line scan is represented by the yellow arrow in the HAADF image. It is observed in the line profile that the distribution of counts of the Cu and Au atoms is almost similar. However, the individual counts of Cu atoms are more all throughout the film compared to Au. Although, the drop in the counts of the both Cu and Au atoms are observed from the dark layer regions in the multilayers. The gradual drop in the counts of Cu and Au is observed because the specimen was tilted to 20^{0} in order to face the STEM-HAADF detector.

Figures 4.4(a-c) represents the high-resolution phase contrast images obtained from the 40TCu specimen. These images are acquired from various regions in the upper thick layer showing strong crystallographic contrast (cf. Figure 4.2a) in the multilayered film. The dotted square boxes (1-3) in the figures 4.4(a-c) depict the presence of some domains with

two dimensional lattice fringes. This indicates that each of these domains is oriented along a particular zone axis. The size of these domains are ~ 2-6 nm. In order to identify the structures associated with these domains, the regions in the square boxes (1-3) have been cropped and are shown separately in the outsets (1-3). The outset '1' represents the phase contrast image (square box '1') along with its FFT. The values of inter-planar spacings corresponding to the spots in the FFT are ~ 0.216 nm and ~ 0.221 nm. The values of these inter-planar spacings do match with the (211) and (120) planes of the oP8 (AuCu) structure. The simulated diffraction pattern of oP8 structure along [$\bar{2}$ 1 3] zone axis also shows a close match with the FFT as shown alongside. This confirms the presence of this intermetallic phase in the multilayer. The direct structure of oP8 overlaid onto the phase contrast image (outset'1') reveals that the bright spots are the clusters of Au and Cu atoms. This information enabled us to construct a nanocluster (27 unit cells) for oP8 phase existing in the same domain. The oP8 phase is projected along [$\bar{2}$ 1 3] direction with an upward vector [0 1 0]. The 211 and 120 planer facets can be observed at the surface of this nanocluster. Similarly, the outset '2' represents the phase contrast image (square box '2') along with its FFT. The values of inter-planar spacings corresponding to the spots in the FFT are ~ 0.222 nm and ~ 0.223 nm respectively. The values of these inter-planar spacings do match with the ($\bar{1}$11) and (111) planes of tP4 (AuCu) structure. The simulated diffraction pattern of tP4 structure along [0 1 $\bar{1}$] zone axis also shows a close match with the FFT as shown alongside. This confirms the presence of this intermetallic phase in the multilayer. The direct structure of tP4 overlaid onto the phase contrast image (outset '2') reveals that the bright spots represent the columns of Au and Cu with mixed chemistry.

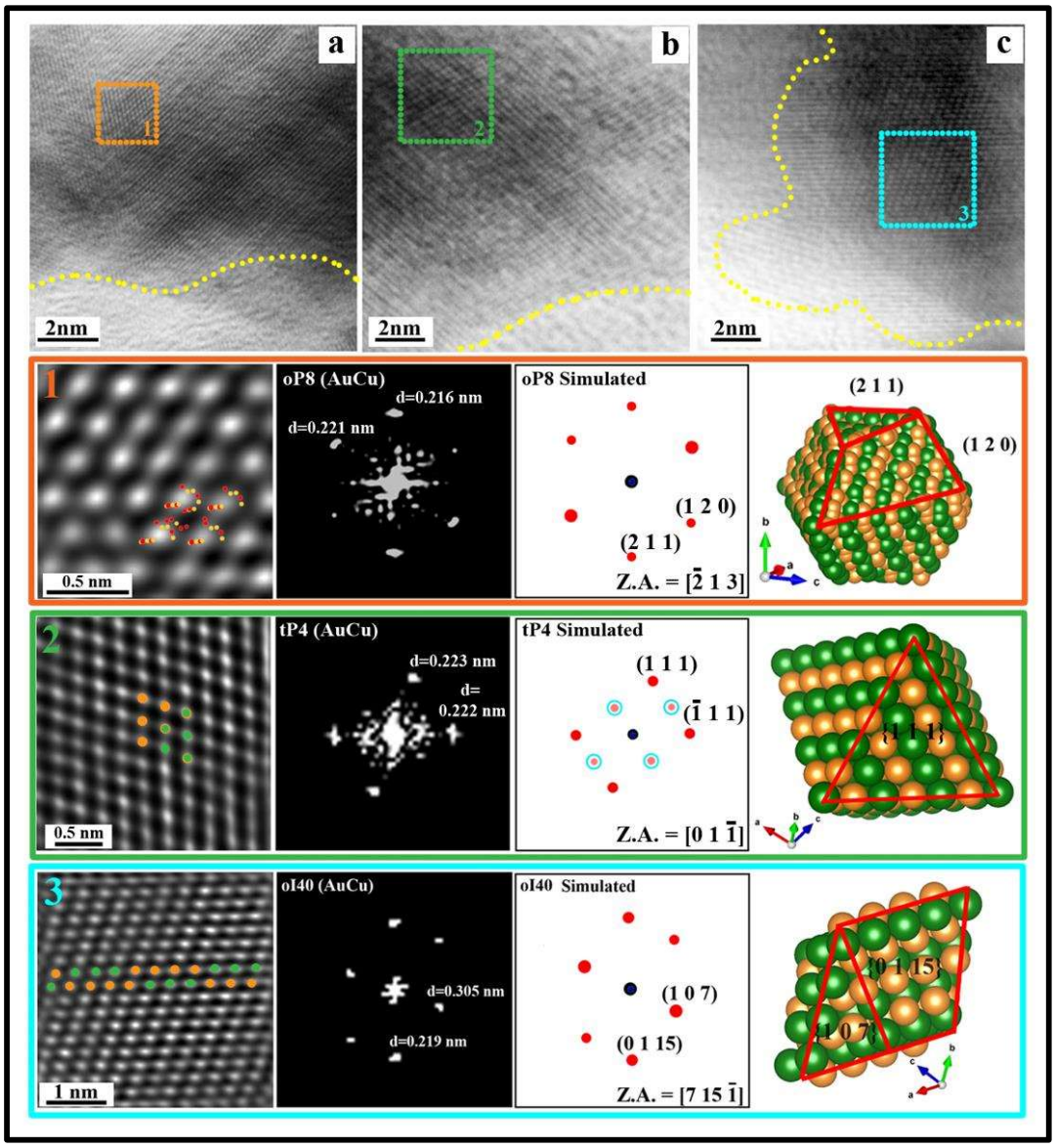

Figure 4.4: *Atomically resolved phase contrast images obtained from the few regions within the multilayer of 40TCu specimen* ***(a-c)****. Square box '1'(orange color) in* ***(a),*** *depicts 2-D lattice fringes. Multislice simulated image of square box '1' along with structure (oP8) overlay is shown in the outset '1'. Also, FFT from the same region with its corresponding simulated diffraction pattern and simulated nanocluster (27 unit cells) for oP8 structure is shown alongside. Square box '2'(green color) in* ***(b),*** *depicts 2-D lattice fringes. Multislice simulated image of square box '1' along with structure (tP4) overlay is shown in the outset '2'. Also, FFT from the same region with its corresponding simulated diffraction pattern*

and simulated nanocluster (27 unit cells) for tP4 structure is shown alongside. Square box '3'(cyan color) in ***(c),*** *depicts 2D lattice fringes. Multislice simulated image of square box '3' along with structure (oI40) overlay is shown in the outset '3'. Also, FFT from the same region with its corresponding simulated diffraction pattern and simulated nanocluster (27 unit cells) for oI40 structure is shown alongside.*

This information enabled us to construct a nanocluster (27 unit cells) for tP4 phase existing in the same domain. The tP4 phase nanocluster as projected along [0 1 $\bar{1}$] direction with an upward vector [111] is shown alongside outset '2'. The 111 type planer facets can also be observed at the surface of this nanocluster. The outset '3' represents the phase contrast image (square box '3') along with its FFT. The values of inter-planar spacings corresponding to the spots in the FFT are ~ 0.305 nm and ~ 0.198 nm. The values of these inter-planar spacings do match with the (0 1, 15) and (107) planes of oI40 (AuCu) structure. The simulated diffraction pattern of this oI40 structure along [7, 15 $\bar{1}$] zone axis also shows a close match with the FFT as shown alongside. This confirms the presence of this intermetallic phase in the multilayer. The direct structure of oI40 overlaid onto the phase contrast image (outset '3') reveals that the bright spots are columns of Au and Cu with mixed chemistry. This information enabled us to construct a nanocluster (27 unit cells) for oI40 phase existing in the same domain. The oI40 phase nanocluster as projected along [7, 15 $\bar{1}$] direction with an upward vector [0 1 0] is shown alongside this outset '3'. The {0 1, 15}and {1 0 7} type planer facets can also be observed at the surface of this nanocluster.

4.4 Discussion

The entire investigation onto the 40TCu and 40TAu specimens at different length scales brings out interesting information about microstructure and phase evolution. Such

investigations have also been done earlier on the other thin films [22,45,180,268]. Reversing the sequence of the layers is the key to understand the architectural dependence of phase and microstructure in the multilayer, which is likely to influence the functional properties in interconnects, plasmonics, catalysis etc. [118,177,179,227,268]. It has been reported in literature that a small fluctuation in the inter-diffusion distance may lead to the change in the behavior of multilayers [43,48,106,269,270]. In our investigation, a difference of ~2 nm has been observed in the inter-diffusion distance amongst 40TCu and 40TAu multilayer thin films (cf. Figures 4.2a and 4.2b). The change in surface roughness is also observed on comparing both the multilayers. The 40TAu surface is rougher than 40TCu multilayer as the number of undulations over about ~100 nm distance is higher in case of 40TAu (Figures 4.2a and 4.2b). The rough surface of the thin films leads to higher noise in the profile measurements [44,118]. The chemical investigation of these two multilayer specimens done through STEM-EDS mapping reveals that both the multilayers are primarily Au and Cu based solid solutions (Figure 4.3a,b). However, at the intermediate layer, where the extensive inter-diffusion has taken place, appears to be Cu rich. This investigation suggests that even on reversing the multilayer sequence, the overall chemistry remains unaltered when deposited through thermal evaporation technique. Only, the diffusion of Cu towards the Si substrate could be observed in case of 40TAu (Figure 4.3a (HAADF)). The uniformity in composition of the multilayers irrespective of the deposition sequence is considered to be advantageous [20,59,138,271]. Additionally, the investigations based on the HRTEM results reveals that the 40TCu multilayer consists of amorphous/ crystalline interfaces (Figure 4 (a-c)). These interfaces are created wherever the diffusion couple has formed [51]. The earlier investigations, as reported in literature [157,207,272,273], have shown that such kind of amorphous/crystalline interfaces are

desirable for better plasmonic and catalysis properties. In addition to this, such amorphous/crystalline composite nature helps in maintaining the mechanical integrity of the multilayer thin films [124]. Differently oriented crystalline domains with oP8, tP4, oI40 structures (figure 4 insets (1-3)) are observed within the crystalline multilayers.

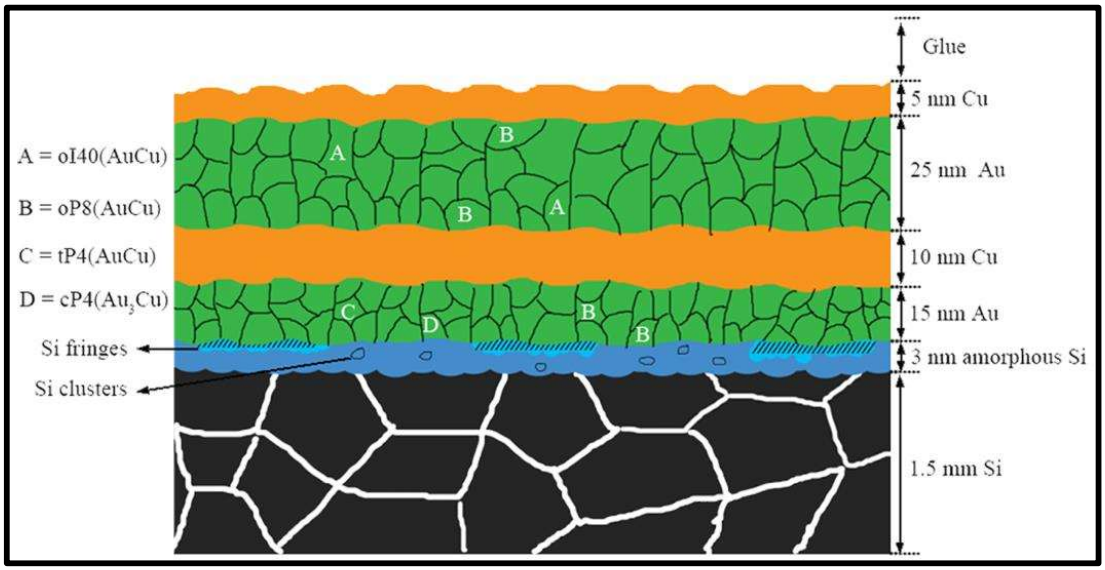

Figure 4.5: *Schematic representation of the microstructure and interface of the Au/Cu multilayered thin film cross-section of 40TCu specimen.*

With the help of multislice image simulation, nanoclusters have been generated in order to show the facets with which the intermetallic phases grow after nucleation. The presence of AuCu intermetallics with faceted morphology has been proved to show improved plasmonic and catalysis properties. [65,126].

The presence of facets, which has a direct correlation with the surface-to volume ratio play a key role in improving the properties [53,61]. However, the presence of intermetallic phases in Au-Cu alloy/multilayer is not considered good for its application in microelectronic industries as interconnects [179,183]. Formation of intermetallics increase the noise to signal ratio by disturbing the electron transport properties.[42,87,95,179]. For

microelectronics and packaging industries solid solution of Au-Cu alloy is considered beneficial [65]. Detailed HRTEM investigations and multislice simulations had been done on the 40TAu specimens in our earlier study and reported in chapter 3 [42]. There also the same intermetallic phases were observed, but with different facets. The mechanism for the evolution of these intermetallic phases in both the multilayers (40TAu and 40TCu) appears to be similar. Instantaneous process and structural parameters such as strain, defects, extent of intermixing, adatom mobility etc., leads to the formation of different intermetallic phases. Referring to figure 4.1, peak broadening in the experimental curve for 40TCu specimen can be manifested to the small grain size and presence of local strain (non-uniform). Whereas, peak splitting is due to the presence of two or more phases. In order to accommodate the local strain, any structure tries to expand or contract itself along a certain axis [113]. Such structural transformations give rise to intermetallics formation. Attenuation of defects is another way of reducing the local strain [39]. In this process also, the ordered structures are formed, if the defects are configured (minimum energy) in such a manner, they would result in the order-disorder transformation [110]. During thin film deposition, the coalescence of atomic clusters happens and that depends on the adatom mobility [4]. Extent of intermixing of atoms relies on such phenomena. Atomic level intermixing at interfaces is also one of the crucial factors for the growth of intermetallics [5,42]. The schematic view of the cross section of the multilayer is given in figure 4.5. In the figure, morphology and structure of the phases as obtained from the electron microscope observation are given along with their dimensions.

4.5 Conclusions

The change of deposition sequence onto a polycrystalline Si substrate for 40TCu vis-à-vis that of 40TAu has led to a change in their microstructures. The film/substrate interface is

amorphous/crystalline in case of 40TAu whereas it is crystalline /crystalline in the 40TCu specimen. The only similarity in them is, both the multilayers consist of the amorphous/crystalline interface at its intermediate region. The 40TAu mutlilayer film is more strained as more undulations are present on the top surface. Columnar morphology is observed in both the multilayer specimens. The inter-columnar boundary density is related to the diameter to thickness ratio. The chemistry of the multilayers is found to be unaltered with the deposition sequence. The evolution of intermetallic phases such as oP8, tP4 and oI40 along with the solid solution phase is also akin to that of 40TAu specimen. Formation of all these phases is attributed to the existence of competing energy minima. This has been mentioned in chapter 3.